

PAPER • OPEN ACCESS

Source term calculation and validation for ^{18}F -production with a cyclotron for medical applications at HZDR

To cite this article: J Konheiser *et al* 2019 *J. Radiol. Prot.* **39** 906

View the [article online](#) for updates and enhancements.




BERTHOLD

Fast and reliable detection
of any increase in dose rate
in the workplace

[Learn more](#)

Source term calculation and validation for ^{18}F -production with a cyclotron for medical applications at HZDR

J Konheiser^{1,4} , S E Müller¹, A Magin^{2,3}, B Naumann¹ and A Ferrari¹

¹ Helmholtz-Zentrum Dresden-Rossendorf, D-01328 Dresden, Germany

² Karlsruhe Institute of Technology (KIT), D-76131 Karlsruhe, Germany

E-mail: j.konheiser@hzdr.de

Received 7 March 2019, revised 3 June 2019

Accepted for publication 19 June 2019

Published 21 August 2019



CrossMark

Abstract

In this document we present the calculation and experimental validation of a source term for ^{18}F -production with a cyclotron for medical applications operating at 18 MeV proton energy and 30 μA proton current. The Monte Carlo codes MCNP6 and FLUKA were used for the calculation of the source term. In addition, the radiation field around the ^{18}O -enriched water target was simulated with the two codes. To validate the radiation field obtained in the simulation, an experimental program has been started using activation samples which are placed close to the water target during an ^{18}F -production run of the cyclotron. After the irradiation, the samples are analysed and the resulting activation is compared to Monte Carlo calculations of the expected sample activation. We find good agreement between simulations and experimental results, with most calculation to experiment (C/E) ratios well between 0.6 and 1.4.

Keywords: cyclotron, neutron measurement, neutron source calculation

(Some figures may appear in colour only in the online journal)

³ Now at: SICK AG, D-79276 Reute, Germany.

⁴ Author to whom any correspondence should be addressed.



Original content from this work may be used under the terms of the [Creative Commons Attribution 3.0 licence](https://creativecommons.org/licenses/by/3.0/). Any further distribution of this work must maintain attribution to the author(s) and the title of the work, journal citation and DOI.

1. Introduction

Positron emission tomography has developed into a standard tool for imaging methods in medicine. The required radionuclides are often produced with the aid of cyclotrons. Depending on the emitter to be produced, different nuclides are bombarded with protons or deuterons that trigger nuclear reactions. In addition to the desired nuclide, neutron and gamma radiation is also produced during these nuclear reactions. These are the main source of the radioactive dose rate on the outside of the protection buildings and determine the shielding design. In addition, neutron radiation leads to the activation of the construction and building materials, which could be important for the decommissioning of the facilities. Therefore, the correct determination of neutron and gamma source terms is the imperative basic condition for a correct shielding calculation and thus for a sufficient protection of the employees.

Several approaches can be taken to obtain the source term needed for the shielding calculations. In one approach, the source term spectrum is determined using nuclear model programs such as ALICE-91 [1], and subsequently, the corresponding transport calculation (shielding calculation) is done using the obtained spectrum. The determination of the absolute number of emitted neutrons is then carried out on the basis of tabulated activities assuming a full absorption of the beam. For many reactions these are available in tabular form for different proton energies and a standard current [2]. This approach for the ^{18}F -production is applied in the source term quoted in the supporting documentation for an ACSI TR-FLEX cyclotron [3], assuming that the neutron source term originates exclusively from the desired reaction. In [4] the energy and angular distributions of the neutron source term were taken from the double differential data of the nearby reaction $^{14}\text{N}(p,n)^{14}\text{O}$, but also basing the absolute number of emitted neutrons on the production rate of ^{18}F . Often the source term can be traced back to a confidential information from the manufacturer of the cyclotron with little information on how it was obtained [5–7].

A different approach which is related to the large progress on radiation transport and reaction codes in recent years consist in the direct calculation of the full neutron and gamma source terms including all contributing reaction channels with the radiation transport codes themselves, often accompanied by comparisons of the simulated results with experimental measurements. Examples for this approach can be found in [8–10].

For the shielding calculations for the new cyclotron with proton beam energies of 24 MeV and 28 MeV at the HZDR [11], this second approach was used. Different nuclear models are integrated into the program MCNP6 [12] to calculate the generation of neutrons in the target. Likewise, the source term can also be determined with the help of corresponding cross section tables. Both possibilities were used. The source terms calculated in this approach show a large difference respect to the values that were obtained using the approach mentioned above on the basis of tabulated activities. A calculation with the FLUKA [13, 14] program gave similar results like MCNP6. These results have been already published and discussed in [11]. To validate the results from independent radiation transport codes, in addition to source term calculations with MCNP6 and FLUKA for HZDR's 18 MeV cyclotron⁵, this work gives experimental results for neutron fluence measurements using activation sample monitors. For these measurements, existing experience from the field of reactor dosimetry was applied.

⁵ Cyclone 18/9 model by IBA.

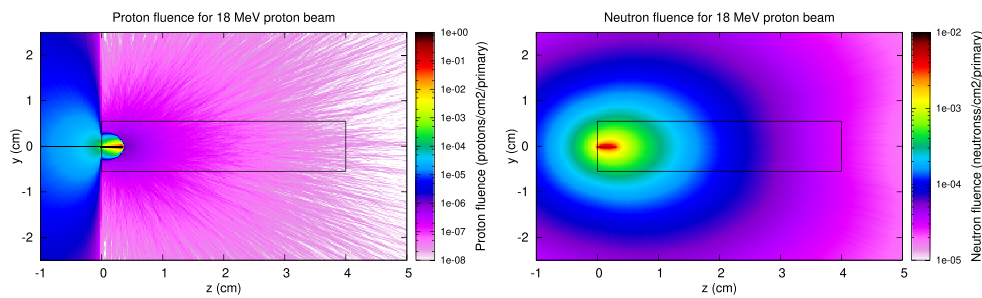


Figure 1. Proton- and neutron fluences per primary proton obtained with FLUKA for 18 MeV protons hitting the ^{18}O -enriched water target.

2. Determination of the neutron source term

To calculate the neutron source term, simulation models were created with both MCNP6 and FLUKA which consist of a cylinder with radius 0.55 cm and a length of 4 cm, filled with water enriched with 97% ^{18}O . These dimensions correspond to typical target bodies used at the IBA cyclotron. The protons' direction is along the cylinder axis, hitting the target on one of the circular base surfaces. The precise shape of the proton beam is not known. Therefore, two approaches were calculated. In the first case the proton beam was simulated as an infinitesimally small pointlike beam and in the second case a circular surface beam with a Gaussian distribution with a standard deviation of 0.125 cm cut off at the target radius was chosen. The two approaches gave identical results (see also [11]). In the following we will use the results obtained with a pointlike proton beam in the simulations. The emitted neutron spectrum is determined on the surface of a surrounding sphere with a radius of 10 m, large enough to minimize geometrical effects due to the target shape. The generation of neutrons in the target was carried out using nuclear physics models of reaction cross sections. In MCNP a cascade exciton model [15] was used, while FLUKA uses a pre-equilibrium cascade model (PEANUT) [16] for the nuclear interactions. In addition, MCNP6 calculations were also carried out with evaluated nuclear data of the (p, n) reaction. Since ^{18}O -data are not included in the standard library of MCNP6, they were generated using the NJOY [17] program and imported into MCNP6. The required reaction cross-sections were read from the nuclear data library TENDL, which is based on the nuclear core model code TALYS [18]. This possibility to use externally generated cross sections does not exist for FLUKA. Since FLUKA does not include neutron cross sections for ^{18}O , cross section data for ^{16}O was used instead for the interactions of neutrons in the water. At thermal energies, the O^{16} total neutron cross section is at maximum 25% higher than the one for O^{18} . In both cases, the cross sections are dominated by the ones for elastic scattering of neutrons. Since the main source of neutrons is the dominating (p, n) reaction at the O^{18} , the influence of the secondary (n, g) , (n, n') and $(n, 2n)$ reactions is very small. Further differences in the calculations consist of the used cross section data libraries. The data libraries ENDF/B-VI.8 [19] were used for the interactions of neutrons with energies below 20 MeV at FLUKA and ENDF/BVII.1 [20] for MCNP6.

In figure 1, both the proton and neutron fluences per primary proton are depicted as obtained with the FLUKA simulation code. The protons penetrate only about 0.5 cm into the water target before they are stopped. The water target absorbs almost all protons in the forward direction, leaving only the backscattered ones to the left of the target. Neutrons are produced along the trajectory of the proton beam in the water. Figure 2 shows the differential neutron rate recorded across the surrounding sphere for 1 μA of proton beam current obtained

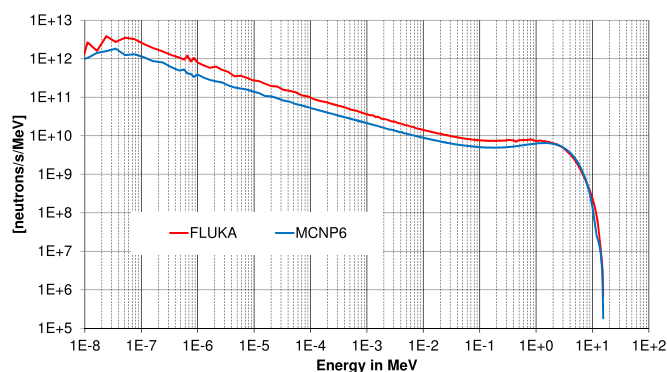


Figure 2. Differential neutron rate for an 18 MeV proton beam with 1 μA hitting the water target. The spectra are available from [21].

with MCNP6 (version 6.1.1) and FLUKA (version 2011.2x). Integrating the spectrum over energy we find a total neutron yield of $3.21 \times 10^{10} \text{ n s}^{-1}$ for 1 μA of proton current for the FLUKA calculation, and $2.99 \times 10^{10} \text{ n s}^{-1}$ for 1 μA of proton current for MCNP6. The higher yield obtained with FLUKA respect to the MCNP6 calculations has already been observed for 24 and 28 MeV protons in [11], and is attributed to differences of the underlying nuclear physics models. The values are about a factor 3 higher than the value of $1.115 \times 10^{10} \text{ n s}^{-1}$ for 1 μA of proton current obtained from [22] for the $^{18}\text{O}(p, n)^{18}\text{F}$ channel. We attribute the difference to additional neutron-producing reaction channels opening at 18 MeV proton energy, as suggested in [23]. It should be noted however that measurements of the neutron yield rate reported in [24] and [25] give results which are close to the value of $1.115 \times 10^{10} \text{ n s}^{-1}$ for 1 μA ⁶.

3. Experimental validation of the radiation field around the target

To validate the calculation of the source terms in section 2, activation monitor foils were placed on top of the irradiation target during a routine run for ^{18}F production. After irradiation, the activation of the foils was measured and compared to predictions from the radiation transport and reaction codes MCNP6 (version 6.1.1) and FLUKA. For these activation studies, a special developer version of FLUKA [26] was used which includes updated information on branching ratios to meta-stable states using the JEFF-3.1A activation library [27] that is not yet available in the official FLUKA version [28].

3.1. Experimental setup to measure the radiation field with sample activation

Figures 3(a) and (b) show the individual activation monitor samples as well as the sample packages and their position on the irradiation container at the cyclotron. The samples consist of different metal foils made of pure metals or alloys. Table 1 shows the monitor samples and the reactions under study with the generated nuclides, the reaction threshold and their half-life. The selected metals are standard monitor materials which are inserted for neutron flux and fluence measurements at fission reactors for power determinations as well as for the

⁶ It was confirmed by the authors of [25] that the values quoted in their document need to be corrected by a factor of 10 and the resulting neutron production yield should therefore read $(1.55 \times 10^{10} \pm 1.03 \times 10^9) \text{ n s}^{-1}$ for 1 μA of beam current. We thank M Hagiwara for this information.



Figure 3. (a) Examples for activation foil samples used in the experiment. (b) The two stacks of activation sample foils in a plastic bag placed on top of the target flange.

Table 1. Composition of the monitor samples with the studied activation reactions and corresponding half-lives.

Monitor sample	Mass fraction	Reactions	Threshold	Half-life
Multi-component	81.63% Ni	$^{58}\text{Ni}(n, np)^{57}\text{Co}$	8 MeV	271.74d
		$^{58}\text{Ni}(n, p)^{58}\text{Co}$	0.4 MeV	70.86d
	15.16% Mo	$^{98}\text{Mo}(n, g)^{99}\text{Mo}$	therm.	66.0h
		$^{100}\text{Mo}(n, 2n)^{99}\text{Mo}$	8 MeV	66.0h
	2.62% W	$^{186}\text{W}(n, g)^{187}\text{W}$	therm.	23.72h
0.26% Mn	$^{55}\text{Mn}(n, g)^{56}\text{Mn}$	therm.	2.58h	
0.31% Au	$^{197}\text{Au}(n, g)^{198}\text{Au}$	therm. (4 eV)	2.69d	
Zinc	100.00% Zn	$^{64}\text{Zn}(n, p)^{64}\text{Cu}$	0.08 MeV	12.70h
		$^{64}\text{Zn}(n, g)^{65}\text{Zn}$	therm.	244d
		$^{68}\text{Zn}(n, g)^{69\text{m}}\text{Zn}$	therm.	13.76h
Indium	99.9% In	$^{113}\text{In}(n, g)^{114\text{m}}\text{In}$	therm.	49.5d
		$^{115}\text{In}(n, 2n)^{114\text{m}}\text{In}$	9 MeV	49.5d
		$^{115}\text{In}(n, n')^{115\text{m}}\text{In}$	0.3 MeV	4.5h
Tin	100.00% Sn	$^{116}\text{Sn}(n, g)^{117\text{m}}\text{Sn}$	therm.	13.60d
		$^{117}\text{Sn}(n, n')^{117\text{m}}\text{Sn}$	0.15 MeV	13.60d
		$^{118}\text{Sn}(n, 2n)^{117\text{m}}\text{Sn}$	9 MeV	13.60d

validation of the results in reactor dosimetry [29]. As can be seen from table 1, several of the materials have reactions starting at different threshold energies. This makes it possible to study different energy regions in the spectrum. The monitor packages were positioned directly on top of the irradiation target in order to achieve a high neutron flux and thus high reaction rates. The irradiation took place during a regular ^{18}F production run. The energy of the protons was 18 MeV with average beam current of $25 \mu\text{A}$ and the irradiation lasted for 50 min.

Two packages with the same stacks of activation monitors were irradiated simultaneously. This allowed independent measurements using two independent laboratories for the

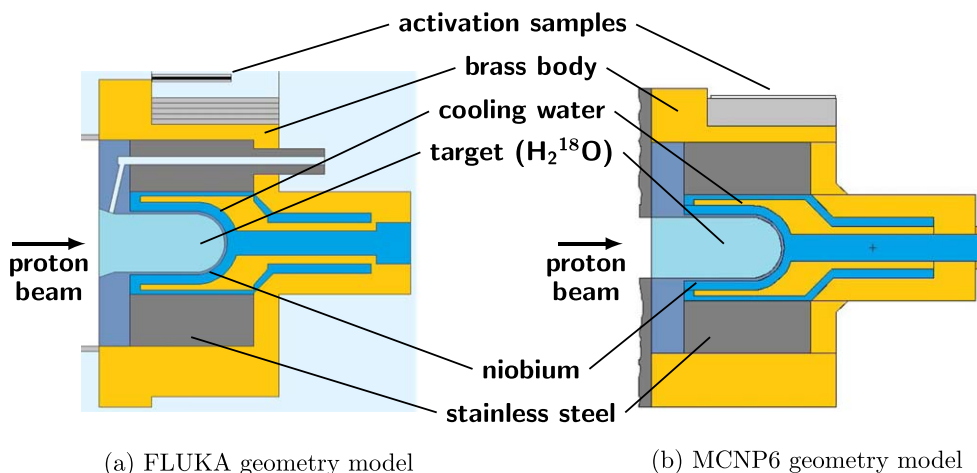


Figure 4. Target geometries for the two simulation codes.

sample activation analysis. The activation measurements were carried out at the ‘Department of Environmental Monitoring’ and at the ‘Laboratory for Environment and Radionuclide Analysis’ of the ‘VKTA—Strahlenschutz, Analytik & Entsorgung Rossendorf e. V.’⁷. The activity was determined by gamma spectrometry using high-purity germanium detectors. Typically, the detectors⁸ have about 44% efficiency relative to a 3" × 3" NaI(Tl) detector, a resolution of 1.78 keV at 1332 keV and are calibrated weekly against a certified standard. In order to detect nuclides with a relatively short half-life, some of the activation monitors were already examined about one hour after the end of irradiation. For some nuclides with longer half-life, the measurements were repeated at longer cooling times and the activity value at the end of irradiation was extrapolated back using the known half-life values. However, it was found in previous studies that these extrapolations were not always reliable, especially when there is a delayed production of a nuclide from an excited state. Therefore both labs were asked to provide the measured values at the time of the measurement and also the values extrapolated back to the time at end of irradiation (EOI). The quoted uncertainties by both laboratories were in the range between 5% and 25%, depending on the reaction channel.

3.2. Calculation of sample activation

Figure 4 shows the geometrical models of the irradiation target chamber created with FLUKA and MCNP6. The construction of the irradiation target was reproduced in great detail. While it is known from which materials the components are made of, precise information on densities and composition was not always available, so standard specifications had to be used. Composition and densities of the materials were implemented identically in the FLUKA and MCNP6 simulations. The beam tube adapter flange and surrounding environment like walls were not implemented in the simulations, on the assumption that the influence of back scattered neutrons is negligible on the activation of the monitors.

The stacks of foil samples were included in the simulations at their corresponding position during the irradiation. Material densities of the samples were measured for each

⁷ VKTA—Radiation Protection, Analytics & Disposal Inc., www.vkta.de.

⁸ Broad Energy HPGe Detector BE5030P by Mirion Technologies, Inc.

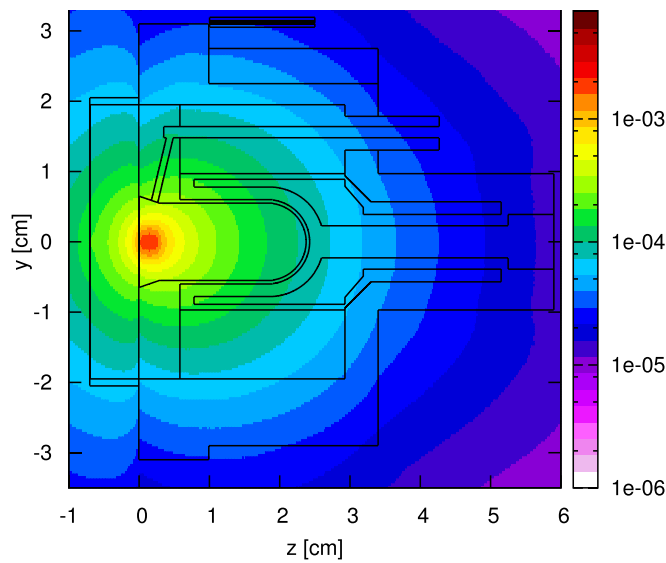


Figure 5. Neutron fluence in neutrons/cm²/primary proton around the target geometry (evaluated with the FLUKA Monte Carlo code).

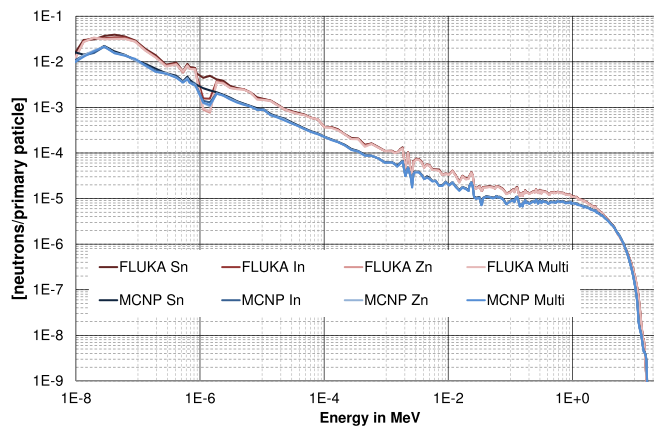


Figure 6. Differential neutron flux per primary proton evaluated with FLUKA and MCNP6.

sample before irradiation, and the average value of the samples of same type was used in the simulation. The source term in the simulations consisted of a point-like proton beam with 18 MeV kinetic energy. Figure 5 shows the neutron fluence on a central vertical section plane as obtained from the output of a FLUKA simulation. One can clearly see the proton stopping peak immediately after the protons enter the ¹⁸O-enriched water and the almost isotropic emission of the neutrons through the target geometry. Figure 6 shows the spectra of neutron flux entering the different samples as calculated by MCNP6 and FLUKA. Similar to figure 2 in section 2, at energies below 1 MeV, the FLUKA values are higher than the MCNP6 values. The strong resonance (at about 1.45 eV) of the absorption cross section for ¹¹⁵In with almost

Table 2. Measured and calculated activities for the multi-component monitor. The measurements for analysis A were done at $t_{\text{meas}} = 6$ h 17 m after EOI, measurements for analysis B were done at $t_{\text{meas}} = 30$ h 13 m after EOI. The uncertainty of the FLUKA values corresponds to the statistical uncertainty. A starred value (*) indicates a C/E ratio which is outside the interval [0.6; 1.4].

Multi-comp. monitor	Measured activity		Simulated activity		Comparison		
	[Bq]		[Bq]		C/E		
Reaction	Analysis	Result	MCNP6	FLUKA	MCNP6	FLUKA	C_M/C_F
$^{58}\text{Ni}(n, np)^{57}\text{Co}$	A	4.2(5)	0.58	0.74(3)	0.14*	0.18*	0.78
	B	4.7(5)	0.58	0.74(3)	0.12*	0.16*	0.78
$^{58}\text{Ni}(n, p)^{58}\text{Co}$	A	330(20)	274	255(1)	0.83	0.77	1.07
	B	455(45)	378	351(2)	0.83	0.77	1.08
^{99}Mo prod.	A	120(8)	72	118(3)	0.60	0.98	0.61
	B	117(12)	56	91.6(2)	0.48*	0.78	0.61
$^{186}\text{W}(n, g)^{187}\text{W}$	A	200(12)	133	239(8)	0.67	1.20	0.56*
	B	106(11)	67	120(4)	0.63	1.13	0.56*
$^{197}\text{Au}(n, g)^{198}\text{Au}$	A	68(4)	41	69(4)	0.60	1.02	0.59*
	B	63(6)	31.4	53(3)	0.50*	0.72	0.59*

30 000 barn is visible in the spectra, except for tin, because the tin sample was placed below the indium sample.

Given the neutron flux rate, the activities $A_i(t_{\text{meas}})$ for each produced nuclide at a time t_{meas} after irradiation in an energy bin i can be determined using the relation

$$A_i(t_{\text{meas}}) = \rho \cdot V \cdot \lambda \cdot \sigma_i \cdot \dot{\Phi}_i \cdot t_{\text{irr}} \cdot (1 - e^{-\lambda t_{\text{irr}}}) \cdot e^{-\lambda(t_{\text{meas}})}. \quad (1)$$

In equation (1), ρ is the density of nuclei in the sample (in nuclei/(barn cm)), V is the sample volume in cm^3 , σ_i is the corresponding reaction cross section in barn for energy bin i , $\dot{\Phi}_i$ is the corresponding neutron flux rate obtained from the simulation in neutrons/ cm^2/s , t_{irr} is the irradiation time in seconds and λ is the decay constant of the reaction product (in 1/s). The total activity is then the sum of the A_i over all energy bins i . Given an irradiation time profile, FLUKA conveniently gives the resulting nuclide activities in Bq cm^{-3} for selected geometry regions at desired times directly in a tabular output. The required cross section data is hard-coded into the FLUKA program and cannot be changed by the user. For MCNP6, equation (1) needs to be applied externally to the simulated neutron flux rates. In this case, the required cross section data had to be generated with the NJOY program. This procedure has the advantage that the neutron flux can be folded over cross sections from different nuclear data libraries. This allows to estimate systematic uncertainties coming from differences between the available cross section data sets. If more than one reaction channel contributed to a measured final state isotope, the resulting activities were added to obtain the final result.

3.3. Discussion of the results

In tables 2–5 the results for the measured and simulated activities for the different monitors at the corresponding time of measurement are presented. Measurements obtained by the ‘Department of Environmental Monitoring’ are reported as ‘Analysis A’ and the ones by the ‘Laboratory for Environment and Radionuclide Analysis’ are reported as ‘Analysis B’. We

Table 3. Measured and calculated activities for the indium monitor. The measurements for analysis A were done at $t_{\text{meas}} = 7$ h 47 m after EOI, measurements for analysis B were done at $t_{\text{meas}} = 27$ h 32 m after EOI. The uncertainty of the FLUKA values corresponds to the statistical uncertainty. A starred value (*) indicates a C/E ratio which is outside the interval [0.6; 1.4].

Indium	Measured activity		Simulated activity		Comparison		
	[Bq]		[Bq]		C/E		
Reaction	Analysis	Result	MCNP6	FLUKA	MCNP6	FLUKA	C_M/C_F
$^{114\text{m}}\text{In}$ prod.	A	29(7)	7	9.9(1)	0.24*	0.34*	0.71
	B	25(3)	6.9	9.7(1)	0.28*	0.39*	0.71
$^{115}\text{In}(n, n')^{115\text{m}}\text{In}$	A	9300(465)	9145	9855(41)	0.98	1.06	0.93
	B	474(47)	434	466(2)	0.92	0.98	0.93

Table 4. Measured and calculated activities for the tin monitor. The measurements for analysis A were done at $t_{\text{meas}} = 26$ h 43 m after EOI, measurements for analysis B were done at $t_{\text{meas}} = 52$ h 35 m after EOI. The uncertainty of the FLUKA values corresponds to the statistical uncertainty. A starred value (*) indicates a C/E ratio which is outside the interval [0.6; 1.4].

Tin	Measured activity		Simulated activity		Comparison		
	[Bq]		[Bq]		C/E		
Reaction	Analysis	Result	MCNP6	FLUKA	MCNP6	FLUKA	C_M/C_F
$^{117\text{m}}\text{Sn}$ prod.	A	84(5)	55.4	66.9(9)	0.66	0.80	0.83
	B	94(9)	52.5	63.5(9)	0.56*	0.68	0.83

Table 5. Measured and calculated activities for the zinc monitor. The measurements for analysis A were done at $t_{\text{meas}} = 24$ h 56 m after EOI, measurements for analysis B were done at $t_{\text{meas}} = 49$ h 27 m after EOI. The uncertainty of the FLUKA values corresponds to the statistical uncertainty. A starred value (*) indicates a C/E ratio which is outside the interval [0.6; 1.4].

Zinc	Measured activity		Simulated activity		Comparison		
	[Bq]		[Bq]		C/E		
Reaction	Analysis	Result	MCNP6	FLUKA	MCNP6	FLUKA	C_M/C_F
$^{64}\text{Zn}(n, p)^{64}\text{Cu}$	A	1200(60)	891	830(8)	0.74	0.69	1.07
	B	242(48)	234	218(2)	0.97	0.90	1.07
$^{64}\text{Zn}(n, g)^{65}\text{Zn}$	A	3.2(7)	1.7	2.26(2)	0.53*	0.71	0.75
	B	2.8(4)	1.7	2.25(2)	0.61	0.80	0.76
$^{68}\text{Zn}(n, g)^{69\text{m}}\text{Zn}$	A	15(1)	6.3	8.3(4)	0.42*	0.55*	0.76
	B	6.3(6)	1.8	2.41(12)	0.28*	0.38*	0.75

have only kept results for reactions for which both laboratories reported a significant value and for which the statistical uncertainty of the simulations was 15% or better. This e.g. excludes the reaction $^{55}\text{Mn}(n, g)^{56}\text{Mn}$ in table 1, for which only Analysis A gave a measured

result. In total 11 measurements for different nuclides remain. Numbers in parenthesis correspond to uncertainties on the last digits. The MCNP6 results in the tables use cross section data from the JEFF3.1A libraries for the Indium, Zinc and Tin monitors, while for the multi-component monitor ENDF/B-VII.1 were used (except for the $^{58}\text{Ni}(n, p)^{58}\text{Co}$ reaction, for which also JEFF3.1A libraries were used).

Table 2 gives the results for the multi-component monitor. The two analyzes A and B were done with a time difference of 24 h in the two different labs. Except for the $^{58}\text{Ni}(n, np)^{57}\text{Co}$ reaction, the FLUKA code reproduces the experimental results reasonably well, with calculation-over-experiment (C/E) values between 0.77 and 1.20. MCNP6 gives results which are lower than the FLUKA ones by 20%–40%, except for the ^{58}Co production, in which MCNP6 results give slightly better C/E ratios than FLUKA results. The lower values obtained with the MCNP6 code respect to the FLUKA results are consistent with the results on the source term in section 2, in which the MCNP6 results below 1 MeV are 40%–50% lower than the ones obtained with FLUKA. Both simulation codes consistently predict activities which are too low by factors 5–8 for the $^{58}\text{Ni}(n, p)^{57}\text{Co}$ channel, while the experiments agree within errors (the long half-life of ^{57}Co of 270 d allows to compare the measurements directly). An interesting fact is that the activity due to ^{58}Co is larger for analysis B. This is due to the fact that there is a delayed production of ^{58}Co due to the presence of the meta-stable state $^{58\text{m}}\text{Co}$ which decays with a half-life of 9 h to ^{58}Co . This is taken care of in the simulations, but not in the extrapolation of the measurements back to the end of irradiation. For this reason it was decided to compare the simulations with the experimental results at the time of measurement.

For the results of the indium monitor in table 3, we find that both codes predict a factor 3–4 less activity for the production of $^{114\text{m}}\text{In}$, but are remarkably close to the measurements for the channel $^{115}\text{In}(n, n)^{115\text{m}}\text{In}$.

The results for the production of $^{117\text{m}}\text{Sn}$ with the tin monitor are given in table 4. The results with the FLUKA code give C/E ratios of 0.80 and 0.68, with the MCNP6 results being 17% lower in both cases.

Table 5 gives the results for the zinc monitor. For the channel $^{64}\text{Zn}(n, p)^{64}\text{Cu}$, MCNP6 gives results which have a C/E ratio of 0.74 for analysis A and 0.97 for analysis B, with FLUKA results being consistently 7% lower. The activity due to the reaction $^{64}\text{Zn}(n, g)^{65}\text{Zn}$ is simulated by the FLUKA code with C/E ratios of 0.71 for analysis A and 0.80 for analysis B, while for the channel $^{68}\text{Zn}(n, g)^{69\text{m}}\text{Zn}$ FLUKA predicts values significantly lower than the experimental results, namely a C/E ratio of 0.55 for analysis A and 0.38 for analysis B. For both reactions, MCNP6 predictions are about 25% lower than the FLUKA predictions.

In summary, for most of the reactions, the FLUKA code gives results with C/E ratios between 0.68 and 1.20, with the MCNP6 calculations giving in general results which are 10%–40% lower (with the exception of the $^{64}\text{Zn}(n, p)^{64}\text{Cu}$ and the $^{58}\text{Ni}(n, p)^{58}\text{Co}$ reaction, for which MCNP6 results are 7%–8% higher than the FLUKA results).

Both codes consistently give lower results for the production of $^{114\text{m}}\text{In}$ and the channel $^{68}\text{Zn}(n, g)^{69\text{m}}\text{Zn}$, with C/E ratios between 0.34 and 0.55 for FLUKA results and 0.24 and 0.42 for MCNP6 results. An especially large deviation between simulation and measured values is found for the reaction $^{58}\text{Ni}(n, np)^{57}\text{Co}$ channel, with C/E ratios 0.16 and 0.18 for the FLUKA results and 0.12 and 0.14 for results obtained with MCNP6. Again, for these three channels, the MCNP6 results are lower than the FLUKA results by 20%–30%.

3.4. Uncertainties in the calculations

To estimate the uncertainties on the calculations, we need to address the different terms in equation (1). The primary sources of uncertainties in the simulations are the neutron flux rate at the sample position and the reaction cross sections. The neutron flux rate depends on the calculation of the source term (and therefore the underlying model for proton-induced neutron production in the water target), the proton beam current and to some extent the modeling of the target geometry. As mentioned in section 3.2, the geometry of the system has been implemented with great care. The two geometric models differ only in minor details (see figure 4), and contain both identical material compositions and densities. We therefore consider systematic effects from the geometry negligible when comparing the two simulations, and also they are thought to have a minor effect when comparing simulation results to the measurement, even given the fact that the influence of possible backscattering of neutrons from surrounding walls was not considered. The neutron flux rate scales linearly with the proton beam current, and a deviation of the current from the nominal value of 25 μA will reflect on the neutron flux rate. However, the beam parameters can be determined very well and their uncertainties are very small. The dominant effect comes from the uncertainty of the source term—as can be seen from figure 2 this can reach up to 50% below energies of 1 MeV, and is certainly the reason why the MCNP6 results for most channels are significantly lower than the ones from FLUKA. A hint at the size of the uncertainty (which is energy dependent) is given by the C_M/C_F -values in tables 2–5. As can be seen, it can reach up to 40% and more in some cases.

Fundamental for the determination of the reaction rates are the data libraries used in the evaluations. Different evaluated nuclear data libraries are available for the majority of nuclides at e.g. NEA [30]. For some nuclides only data calculated from theoretical models is available. Using MCNP6's capability to include different cross section data sets, we have studied the effects of different cross sections on the simulation calculations. The cross section data was generated with the use of the NJOY program. Among the libraries tested were ENDF/B-VII, JEFF3.1A, JENDL33, EAF2010 and ROSFOND2010. If branching fractions for isomeric states were given, these were considered. While for some of the considered reactions (like $^{115}\text{In}(n, n')^{115\text{m}}\text{In}$, $^{117\text{m}}\text{Sn}$ production and $^{197}\text{Au}(n, g)^{198}\text{Au}$), the different libraries gave consistent results, in some cases discrepancies on the order of 30%–40% could be observed (^{114}In production and the $^{68}\text{Zn}(n, g)^{69\text{m}}\text{Zn}$ reaction). As an example, in figure 7 the evaluated cross section for the $^{68}\text{Zn}(n, g)^{69}\text{Zn}/^{69\text{m}}\text{Zn}$ reaction is shown obtained from two different data libraries (JEFF3.1A and the ENDF/B-VII). It can be seen that while for thermal energies, the cross sections are in good agreement, at high energies and around the first large resonance, the ENDF/B-VII data gives higher values, resulting in an activation result which is about 30% higher than the one calculated with the JEFF3.1A data. For the remaining reactions, the differences in the activation results due to the use of different cross section data sets is on the order of 10%.

Another point is the influence of the energy group structure. While the FLUKA code uses a fixed 260 energy groups structure, one can have a larger number of groups for the cross section data sets generated with NJOY for MCNP6. For the reaction $^{58}\text{Ni}(n, p)^{58}\text{Co}$ activities were calculated based on ENDF/B-VII.1 data determined with a 260 and 640 energy group structure. One finds an effect of 10% towards a better agreement with the experiments using the high-resolution structure. This shows a general problem in the calculation of group-wise cross-sections. These may be underestimated in some cases, especially for threshold reactions. Generally, the flux decreases in the high energy region but

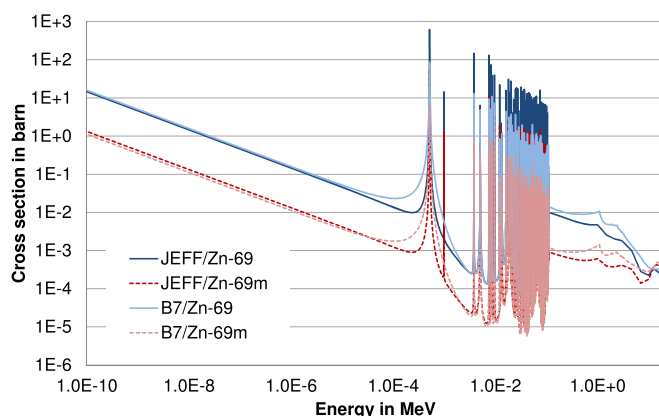


Figure 7. Evaluated cross sections for the reaction $^{68}\text{Zn}(n, g)^{69\text{m}}\text{Zn}$ as obtained with the JEFF3.1A and the ENDF/B-VII data libraries.

cross-sections increase very strongly. Therefore it is very important to resolve the upper energy range well.

The volumes of the monitors in the two sample stacks are not fully identical, the simulation results were calculated using the average volume of two monitors of the same material. While this effect is at maximum 1% for the Indium, Zinc and the multicomponent monitor, it reaches about 5.5% for the Tin monitors (and therefore the simulation results on the $^{117\text{m}}\text{Sn}$ production). Of course, this is negligible compared to the potentially large uncertainties on the neutron flux rate and the cross section spectra.

After the irradiation, we were notified by the operator of the cyclotron that the irradiation had to be stopped for about 10 min due to a vacuum problem. Once the problem was fixed, irradiation resumed to complete the 50 min of irradiation time. Due to the fact that the lifetimes of the produced isotopes in the reactions in table 1 are quite long, we do not expect a large effect due to this interruption. An additional simulation with the FLUKA package using an irradiation time profile of 30 min of beam, followed by 10 min of no beam and finally additional 20 min of beam gave indeed no significant differences within the statistical uncertainties respect to the calculation with a full uninterrupted beam for 50 min.

Finally, the values for material densities ρ and half-life times λ were taken from the literature or are included in the simulation codes and the corresponding uncertainties are considered negligible for the present study.

4. Conclusion and outlook

Inspired by the calculations of a shielding assessment for a new cyclotron bunker, investigations on the neutron source term for the ^{18}F production at a IBA Cyclone 18/9 cyclotron were carried out using the Monte Carlo transport and reaction codes MCNP6 and FLUKA. It was found that below 1 MeV, the MCNP6 code gave a differential neutron rate which is smaller than the one by FLUKA by up to 50%. The total neutron production yield for both codes was about 3 times larger than the value obtained from [22] for the exclusive ^{18}F production channel. To validate the results of the Monte Carlo codes, a more realistic model of the target geometry for the Cyclone 18/9 cyclotron was created with the two Monte Carlo codes which was used to calculate the activation of small monitor sample foils made of

different metals and alloys during a typical run of ^{18}F production. These results were then compared to the actual activation of the sample foils after a ^{18}F run which was obtained using gamma spectroscopy with HPGe detectors at two independent laboratories. In total, 11 reactions were investigated, with C/E ratios between 0.6 and 1.4 for most cases. As a general trend, results calculated using the MCNP6 codes were 20%–40% lower than the ones obtained with FLUKA. This may be (partially) explained by the fact that the source term obtained with MCNP6 is lower than the one from FLUKA below 1 MeV. For three reactions, the Monte Carlo simulations were consistently giving much lower results than the measured data (C/E values as low as 0.12 were observed). This was the case for the $^{58}\text{Ni}(n, np)^{57}\text{Co}$ reaction, the production of $^{114\text{m}}\text{In}$ and the reaction $^{68}\text{Zn}(n, g)^{69\text{m}}\text{Zn}$. For these three reactions, the uncertainties discussed can not accommodate the discrepancies, and it is most likely that the underlying cross section data for these reactions is responsible for the results, and eventually this document may help to improve the cross section data base in the Monte Carlo programs in the future.

Despite the uncertainties of the measurements, the obtained results show that the calculation of the neutron source terms with the help of the methods and models which are implemented in radiation transport and reaction codes like MCNP6 and FLUKA should work better for a proton beam of 18 MeV than a calculation based solely on the ^{18}F yield. This is consistent with observations in [23], which reports significantly higher neutron yields for proton energies above 12 MeV for evaluations using a full ALICE-91 calculation respect to evaluations with tabulated yield values for the $^{18}\text{O}(p, n)^{18}\text{F}$ reaction only. However, our observations seem to contradict the experimental results in [24, 25] which find reasonable agreement with the yield of $1.115 \times 10^{10} \text{ n s}^{-1}$ for $1 \mu\text{A}$ of proton current at 18 MeV energy obtained from [22] for the $^{18}\text{O}(p, n)^{18}\text{F}$ channel.

In order to consolidate our results, further experiments will be planned at the new cyclotron of the HZDR. In these experiments, both the target material and the proton energy will be varied. The aim is to provide validated absolute neutron fluence spectra for shielding calculations at medical cyclotrons.

Acknowledgments

The authors would like to thank S Bartel and M Köhler of VKTA for providing the analysis of the sample monitors. We also like to thank S Preusche and F Hobitz of HZDR for assistance and support with the sample irradiation at the cyclotron.

ORCID iDs

J Konheiser  <https://orcid.org/0000-0002-3059-9080>

References

- [1] Blann M 1991 ALICE-91, statistical model code system with fission competition RSIC Code, PACKAGE PSR-146 (Livermore, CA: Lawrence Livermore National Laboratory)
- [2] Gul K 2001 *Charged Particle Cross-section Database for Medical Radioisotope Production: Diagnostic Radioisotopes and Monitor Reactions* IAEA TECDOC 1211 (Vienna: IAEA)
- [3] Advanced Cyclotron Systems 2011 Monte Carlo Simulation of TR 24 Shielding (Sherbrooke Project) documentation supplied with TR-FLEX cyclotron *Final Report* (Richmond, Canada: Advanced Cyclotron Systems, Inc.)
- [4] Sheu R J, Sheu R D, Jiang S H and Kao C H 2005 Adjoint acceleration of Monte Carlo simulations using TORT/MCNP coupling approach: a case study on the shielding

- improvement for the cyclotron room of the Buddhist TZU CHI general hospital *Radiat. Prot. Dosim.* **113** 140–51
- [5] Bosko A, Zhilchenkov D and Reece W D 2004 GE PETtrace cyclotron as a neutron source for boron neutron capture therapy *Appl. Radiat. Isot.* **61** 1057–62
- [6] Bosko A 2005 General Electric PETtrace Cyclotron as a Neutron Source for Boron Neutron Capture Therapy *Dissertation* (College Station, TX: Texas A&M University)
- [7] Facure A and Franca W F 2010 Optimal shielding design for bunkers of compact cyclotrons used in the production of medical radionuclides *Med. Phys.* **37** 6332–7
- [8] Cruzate J A 2015 Estimate of the radiation source term for ^{18}F production via thick H_2^{18}O targets bombarded with 18 MeV protons *Radiat. Phys. Chem.* **117** 54–8
- [9] Benavente J A, Vega-Carrillo H R, Lacerda M A S, Fonseca T C F, Faria F P and da Silva T A 2015 Neutron spectra due ^{13}N production in a PET cyclotron *Appl. Radiat. Isot.* **99** 20–4
- [10] Infantino A *et al* 2016 Assessment of the neutron dose field around a biomedical cyclotron: FLUKA simulation and experimental measurements *Phys. Med.* **32** 1602–8
- [11] Konheiser J *et al* 2016 Source terms, shielding calculations and soil activation for a medical cyclotron *J. Radiol. Prot.* **36** 819–31
- [12] Goorley T *et al* 2012 Initial MCNP6 release overview *Nucl. Technol.* **180** 298–315
- [13] Ferrari A, Sala P R, Fasso A and Ranft J 2005 FLUKA: a multi-particle transport code CERN-2005-10, INFN/TC 05/11, SLAC-R-773
- [14] Böhlen T T, Cerutti F, Chin M P W, Fassò A, Ferrari A, Ortega P G, Mairani A, Sala P R, Smirnov G and Vlachoudis V 2014 The FLUKA code: developments and challenges for high energy and medical applications *Nucl. Data Sheets* **120** 211–4
- [15] Mashnik S and Sierk A 2012 *CEM03.03 User Manual* Report LA-UR-12-01364 (Los Alamos, NM: Los Alamos National Laboratory)
- [16] Ferrari A and Sala P R 1994 A new model for hadronic interactions at intermediate energies for the FLUKA code *Proc. MC93 Int. Conf. on Monte Carlo Simulation in High Energy and Nuclear Physics (Tallahassee, Florida, 22-26 February 1993)* ed P Dragovitsch, S L Linn and M Burbank (Singapore: World Scientific) pp 277–88
- [17] MacFarlane R and Kahler A 2010 Methods for Processing ENDF/B-VII with NJOY *Nucl. Data Sheets* **111** 2739–890
- [18] Koning A J and Rochman D 2012 Modern nuclear data evaluation with the TALYS code system *Nucl. Data Sheets* **113** 2841
- [19] CSEWG-Collaboration 2001 Evaluated Nuclear Data File ENDF/B-VI.8, released in October 2001, <http://nndc.bnl.gov/ndf> (Accessed: 20 May 2019)
- [20] Chadwick M B *et al* 2011 ENDF/B-VII.1 nuclear data for science and technology: cross section, covariances, fission product yields and decay data *Nucl. Data Sheets* **112** 2887–3152
- [21] The data contained in figure 2 is available at <https://doi.org/10.14278/rodare.114> (Accessed: 20 May 2019)
- [22] International Atomic Energy Agency 2001 Charged particle cross-section database for medical radioisotope production: diagnostic radioisotopes and monitor reactions *Report IAEA-TECDOC-1211* Vienna: IAEA
- [23] Carrol L R 2002 Estimating the radiation source term for PET isotope targets *Poster Presentation at the 9th Int. Workshop on Targetry and Target Chemistry (Turku, Finland, 23-25 May 2002)*
- [24] Mendez R, Iiguez M P, Mart-Climent J M, Penuelas I, Vega-Carrillo H R and Barquero R 2005 Study of the neutron field in the vicinity of an unshielded PET cyclotron *Phys. Med. Biol.* **50** 5141
- [25] Hagiwara M, Sanami T, Masumoto K, Iwamoto Y, Matsuda N, Sakamoto Y, Nakane Y and Nakashima H 2011 Spectrum measurement of neutrons and gamma-rays from thick H_2^{18}O target bombarded with 18 MeV protons *J. Korean Phys. Soc.* **59** 2035–8
- [26] FLUKA2 017.0, developer version used with the permission of the FLUKA collaboration
- [27] Forrest R A, Kopecky J and Sublet J-Ch 2002 The European Activation File Cross section Library UKAEA FUS 486 (Brussels, Belgium/Abingdon, Oxfordshire: EURATOM/UKAEA Fusion Association)
- [28] The current officially available version of FLUKA at the time of writing is FLUKA2 011.2x.4
- [29] Konheiser J, Mittag S and Zaritsky S 2009 Neutron fluence calculations for embrittlement surveillance specimens in VVER-1000 *Ann. Nucl. Energy* **36** 1235–41
- [30] Nuclear Energy Agency, <https://nds.iaea.org/exfor/ndf.htm> (Accessed: 20 May 2019)